Cellular Signalling 72 (2020) 109661

Contents lists available at ScienceDirect

Cellular Signalling

journal homepage: www.elsevier.com/locate/cellsig

Fibrin fragment E potentiates TGF-β-induced myofibroblast activation and recruitment

Peder Öhman Fuchs[a,1], Carlemi Calitz[a], Nataša Pavlović[a], François Binet[a], Sara Marie Øie Solbak[b], U. Helena Danielson[b,c], Johan Kreuger[a], Femke Heindryckx[a,*,1], Pär Gerwins[a,d,1]

[a] Dept. of Medical Cell Biology, Uppsala University, P.O. Box 571, SE-751 23 Uppsala, Sweden
[b] Dept. of Chemistry-BMC, Uppsala University, P.O. Box 576, SE-751 23 Uppsala, Sweden
[c] Science for Life Laboratory, Uppsala University, SE-751 85 Uppsala, Sweden
[d] Dept. of Radiology, Uppsala University Hospital, SE-751 85 Uppsala, Sweden

ARTICLE INFO

Keywords:
Fibrosis
Inflammation
Wound healing
Fibrinolysis
Fibroblasts

ABSTRACT

Fibrin is an essential constituent of the coagulation cascade, and the formation of hemostatic fibrin clots is central to wound healing. Fibrin clots are over time degraded into fibrin degradation products as the injured tissue is replaced by granulation tissue. Our goal was to study the role of the fibrin degradation product fragment E (FnE) in fibroblast activation and migration. We present evidence that FnE is a chemoattractant for fibroblasts and that FnE can potentiate TGF-β-induced myofibroblast formation. FnE forms a stable complex with $\alpha_V\beta_3$ integrin, and the integrin β_3 subunit is required both for FnE-induced fibroblast migration and for potentiation of TGF-β-induced myofibroblast formation. Finally, subcutaneous infusion of FnE in mice results in a fibrotic response in the hypodermis. These results support a model where FnE released from clots in wounded tissue promote wound healing and fibrosis by both recruitment and activation of fibroblasts. Fibrin fragment E could thus represent a therapeutic target for treatment of pathological fibrosis.

1. Introduction

The coagulation system is involved in a wide range of inflammatory conditions, such as rheumatoid arthritis [1], scleroderma [2], liver cirrhosis [3] and sepsis [4]. Initially, tissue injury results in the formation of a cross-linked fibrin matrix that creates hemostasis and provides a provisional matrix for wound repair and tissue regeneration. Platelets trapped in the fibrin mesh release chemotactic factors such as platelet-derived growth factor (PDGF-BB), which together with other growth factors, recruits fibroblasts and inflammatory cells [5,6]. The injured tissue is replaced by granulation tissue, which is a collagen rich matrix with fibroblasts and a dense network of new vessels. Upon activation, fibroblasts become contractile myofibroblasts that express α-smooth muscle actin (α-SMA) and secrete large quantities of extracellular matrix proteins, such as collagen I. Myofibroblasts are mainly, but not solely, derived from nearby resting tissue fibroblasts [7] and have been shown to be necessary for normal wound healing [8]. The transition from fibroblast to contractile myofibroblast is mediated by transforming growth factor beta (TGF-β), together with extra domain A containing fibronectin and tensile stress. Myofibroblasts play an essential role in different medical conditions such as fibrosis and chronic inflammatory diseases [9,10]. Myofibroblasts are also major constituents of the tumor stroma, where they likely promote disease progression [11].

Coagulation is initiated by the activation of thrombin, which mediates cleavage of circulating fibrinogen to generate fibrin, which polymerizes to form a dense fibrin meshwork [12]. To accommodate the expanding granulation tissue and the subsequent scar tissue formation, fibrin is continuously degraded by plasmin, generating fibrin degradation products (FDPs) [13,14]. In the clot, each fibrin monomer contains

Abbreviations: α-SMA, α-smooth muscle actin; cRGD, cyclic-RGD peptide EMD 66203; EdU, 5-ethynyl-2′-deoxyuridine; FDPs, fibrin degradation products; FgnE, fibrinogen fragment E; FnDD, D-dimer; FnE, fibrin fragment E; HRP, horse-radish peroxidase; LPS, lipopolysaccharide; PBS, phosphate buffered saline; PBS-T, phosphate buffered saline with 0,1% Tween; PDGF-BB, platelet-derived growth factor; RU, Response units; RGD, arginine-glycine-aspartate; SPR, Surface plasmon resonance; TGF-β, transforming growth factor beta; TIMP1, Tissue inhibitor of metalloproteinases 1; TLR4, Toll-like receptor 4; TMB, 3,3′,5,5′-tetramethylbenzidine

* Corresponding author.
E-mail address: femke.heindryckx@mcb.uu.se (F. Heindryckx).
[1] shared authorship.

https://doi.org/10.1016/j.cellsig.2020.109661
Received 11 December 2019; Received in revised form 19 April 2020
Available online 22 April 2020
0898-6568/ © 2020 The Authors. Published by Elsevier Inc. This is an open access article under the CC BY-NC-ND license (http://creativecommons.org/licenses/BY-NC-ND/4.0/).

a central *E*-domain flanked by one D-domain on each side, and each D-domain is cross-linked to a neighboring D-domain creating a continuous fiber [15]. In order to degrade the clot plasmin is generated by cleaving of the precursor plasminogen. Plasmin cleaves fibrin between the *E*- and D-domain, which generates the FDPs, fibrin fragment E (FnE) and D-dimer (FnDD) [14,16,17]. Patients with chronic inflammatory diseases often exhibit increased serum levels of FDPs, which has been correlated with disease progression and poor prognosis in, for instance liver cirrhosis [3,18], systemic scleroderma [19] and pulmonary fibrosis [20]. Fibrin degradation products have been shown to have biological effects *in vitro* [21,22] as shown by experiments using endothelial cells [22,23], macrophages [24], vascular smooth muscle cells [21,22,25] and leukocytes where they increase cell migration [21,23,25], inflammatory response [24], proliferation and differentiation [23] and regulate survival and apoptosis [23]. However, the effects of FnE on fibroblast migration and activation into myofibroblasts have not been investigated previously.

In this study we show that FnE is a chemotactic factor for fibroblasts and that FnE potentiates TGF-β-induced myofibroblast activation and induces a profibrotic response when infused in the skin of mice. These results show the importance of the coagulation cascade in wound healing and fibrosis, which could be therapeutically relevant for patients with pathologic inflammatory conditions.

2. Materials and methods

2.1. Cell culture and reagents

Rat kidney fibroblasts (NRK−49F, ECACC), human fetal lung fibroblasts (HFL1, ECACC) and immortalized human foreskin fibroblasts (BJ hTERT) were routinely cultured in MEM supplemented with non-essential amino acids, 25 mM HEPES (Sigma), 10% FBS (Gibco), 2 mM glutamax (Gibco) and 1 mM sodium pyruvate (Gibco). Cells were cultured at 37 °C in a humidified atmosphere containing 5% CO_2. Growth medium without FBS was used for starvation, stimulation and cell migration experiments.

For experiments where cells were stimulated, cells were first detached using trypsin-EDTA (Gibco), thereafter resuspended in growth medium and plated at a density of 5×10^3 cells/cm^2. Cells were allowed to attach for 24 h before being starved for 24 h where after fresh starvation medium containing TGF-β and/or FDPs and inhibitors were added. Cells were harvested at indicated times for RNA or protein extraction. RNA was isolated using Total RNA Kit I (EZNA). For protein extraction, the cells were lysed either in protein lysis buffer (150 mM NaCl, 20 mM Hepes, 10% glycerol and 1% NP-40) or directly in SDS-containing sample buffer (see SDS-PAGE and western blot), both solutions containing 100 U/ml aprotinin, 1 mM Pefablock, 2.5 mM EDTA and 100 nM sodium vanadate was added. TGF-β was added at 5 ng/ml, and FDPs at 2 nM unless otherwise indicated. The inhibitors, SB431542 and the cRGDfV peptide EMD 66203 (both from Sigma-Aldrich) were added 30 min prior to stimulation.

2.2. Fibrin gel degradation

HFL1 cells were detached by trypsin-EDTA, resuspended in serum free MEM and pelleted by centrifugation to remove the trypsin. The pellet was resuspended in serum free MEM containing 2.5 mg/ml bovine fibrinogen (Sigma) and, for some conditions, 50 U/ml aprotinin. Recombinant human thrombin (1 U/ml, Sigma) was added to the bottom of a 3.0 μm costar polycarbonate transwell membrane insert (Corning) and HFL-1 cells suspended in 500 μl fibrinogen solution was added to the insert, mixed, and allowed to polymerize for 1 h at 37 °C. After polymerization, serum-free MEM was added on top of the gel. The inserts were after 6 h transferred to new wells containing pre-starved HFL1 cells and left overnight before indicated factors was added to the lower well. Aprotinin was added to maintain final concentration of 50 U/ml. Cells in the lower well were harvested 48 h post stimulation.

2.3. Electroporation of cells for siRNA transfection

HFL1 cells were detached using trypsin-EDTA solution (Gibco) and approx. 600,000 cells pelleted and resuspended in 100 μl transfection solution (Mirus Bio) containing 400 pg targeting siRNA or non-targeting control siRNA. The cell suspension was transferred to an electroporation cuvette (Mirus Bio) and electroporation was carried out using the Nucleofector I (Amaxa) program T-23 or S-05. After electroporation, the cells were divided and seeded equally into 3 wells in a 6-well plate. Cells were allowed to settle for 6–8 h before being starved overnight in serum-free medium. Stimulation with the indicated factors was initiated 48 h before harvest (at 72 h post transfection). Silencer select siRNAs (Ambion) were targeting either *ITGB3* (integrin β3, siRNA id s7580 and s7582), *ITGB5* (integrin β5, siRNA id s7590 and s7589) or *BAMBI* (siRNA id s24523). Negative control siRNA #1 (AM4635) was used as non-targeting control.

2.4. SDS-PAGE and western blot

Protein lysates in lysis buffer were mixed with 2× sample buffer (0.1 M Tris, 10% glycerol, 2% SDS, 5% β-mercaptoethanol and 50 μg/ml bromophenol blue) and heated to 95 °C for 5 min before being loaded onto a 10% polyacrylamide gel. After separation, the proteins were transferred to an Immobilon-Fl membrane (Millipore). The membrane was blocked after transfer using the Odyssey blocking buffer (Licor) diluted 1:4 in phosphate buffered saline (PBS), and then incubated sequentially with primary and secondary antibodies. After primary and secondary antibody incubation the membrane was washed 3 × 15 min in PBS-T (Phosphate buffered saline (Gibco), 0.1% Tween-20). Primary antibodies used were mouse anti-α-SMA (clone 1A4, Sigma-Aldrich) 1:10000, rabbit anti-β-actin (ab8227, Abcam) 1:5000, mouse anti-PARP1 (BD-bioscience) 1:1500, mouse anti-integrin β3 (13166S, Cell signaling) 1:500, rabbit anti-integrin β5 (H00003693, Abnova) 1:250, all added in blocking buffer with 0.1% Tween-20. Secondary antibodies used were: goat-anti-mouse alexa 680 (Invitrogen) and goat-anti-rabbit IRDye 800 (Rockland) 1:20000 diluted in blocking buffer with 0.1% Tween-20 and 0.01% SDS. All incubations were carried out at room temperature for 1 h or overnight at 4 °C. The membranes were scanned using an Odyssey scanner (LI-COR Biotechnology) and band intensities quantified using the Odyssey 2.1 software and normalized to the β-actin signal in each sample.

2.5. Enzyme-linked immune sorbent assay

Protein was extracted using RIPA buffer (R0278, Sigma-Aldrich) and brought to the same concentration after measuring total protein levels using a Pierce BCA protein assay kit (23,225, ThermoFisher). Tissue inhibitor of metalloproteinases 1 (TIMP1) levels were measured in protein lysates and medium samples using a human TIMP1 SimpleStep ELISA (ab187394, Abcam), following manufacturer's guidelines. Shortly, 50 μl lysate or diluted (1:6) was added to the appropriate wells of a 96-well plate coated with an anti-tag antibody, followed by one-hour incubation with 50 μl antibody cocktail. This causes the entire complex (capture antibody, analyte and detector antibody) to become immobilized *via* immunoaffinity of the anti-tag antibody coating on the wells. After washing of the unbound material, a colorimetric reaction is induced using a horse-radish peroxidase (HRP) driven 3,3′,5,5′-tetramethylbenzidine (TMB) color development. The colorimetric signal was measured at 450 nm using a plate-reader.

Transforming growth factor beta levels were determined in protein lysates and medium samples using a TGF-β human mouse uncoated ELISA kit (88–8350-88, ThermoFisher), following manufacturer's guidelines. A 96-well plate was coated with 100 μl per well of capture antibody by overnight incubation at 4 °C. To activate latent TGF-β to

the immune-reactive form, the samples were acidified using 1 N HCL, followed by a neutralizing reaction with 1N NaOH. After washing and blocking of the wells, 100 µl of activated sample was added to the appropriate wells and incubated overnight at 4 ˚C to ensure maximum sensitivity. A biotin-conjugated anti-TGF-β detection antibody was then added to the wells and after washing, a colorimetric reaction was induced by using an HRP-driven TMB color development. The colorimetric signal was measured at 450 nm using a plate-reader.

Activation of NFkB was measured using an ELISA-based method for detecting p65 DNA-binding activity in nuclear extracts (Abcam, ab133112), following the manufacturer's guidelines. Nuclear extracts were obtained using a Nuclear Extraction kit (Abcam, ab1113474) and incubated for one hour on a 96-well plate which contains an immobilized NFkB response element. NFkB from the nuclear extracts will bind to the NfKB response element and is detected using an antibody against NFkB p65. An HRP-conjugated secondary antibody is then added and NFkB activation is measured with a colorimetric plate-reader at 450 nm.

2.6. RT PCR and qPCR

Total RNA was extracted using the Total RNA Kit I (EZNA) and cDNA synthesis was carried out using iScript (Biorad) according to the manufacturers instructions and using 300 ng total RNA for each sample.

Real-time quantitative PCR (qPCR) was performed using Ssofast Evagreen (Biorad) on a mini Opticon machine (Biorad). Data was analyzed using Bio-rad CFX manager software using the ddCt method and normalized to beta actin. The primer sequences used were hsa *ACTB* (β-actin) 5′-forward TCTACCAATGAGCTGCGTGTG-3′, hsa *ACTB* reverse 5′-AGCCTGGATAGCAACGTACA-3′, hsa *ACTA2* (α-smooth muscle actin) forward 5′-TTCAATGTCCCAGCCATGTA-3′, hsa *ACTA2* reverse 5′-GCAAGGCATACCCTCATAG-3′, hsa *COL1A1* (collagen IαI) forward 5′-GATGGACAGCCTGGTGCT-3′, hsa *COL1A1* reverse 5′-ACC AGGTTCACCGCTGTTAC-3′, hsa *COL3A1* (collagen IIIαI) forward 5′—3′, hsa *COL3A1* reverse 5′—3′, hsa *FN* (fibronectin) forward 5'-TTTGTGGTCTCCTGGGTCTC-3′, hsa *FN* reverse 5′-AGAAGTGGCTGTG CTTGGAA-3′, ED-A containing hsa *FN* forward 5′-AATCCAAGCGGAG AGAGTCA-3′, ED-A containing hsa *FN* reverse 5′-GGTCACCCTGTACC TGGAAA-3′, hsa *ITGB3* (integrin β3) forward 5'-ATGGGGACACCTGT GAGAAC-3′, hsa *ITGB3* reverse 5′-ACGCTTGCAGGTATTTTCG-3′, hsa *ITGB5* (integrin β5) forward 5′-GCCTTGCTTGGAGAGAAAT-3′, hsa *ITGB5* reverse 5′-AATCTCCACCGTTGTTCCAG-3′. hsa *BAMBI* forward 5′-ATCGCCACTCCAGCTACATC-3′, hsa *BAMBI* reverse 5′-GGCAGCATC ACAGTAGCATC -3′.

2.7. EdU proliferation assay

The proliferation assay was carried out in medium containing 2% FBS. Cells were incubated with 1 µM 5-ethynyl-2′-deoxyuridine (EdU, Invitrogen) for 6 h (42–48 h post stimulation) before fixation in 4% PFA in PBS for 15 minutes at room temperature. EdU incorporation was visualized using the Click-iT™ EdU Alexa Fluor® 488 or 555 Imaging Kit (Invitrogen), using Hoechst 33342 as nuclear staining, according to the manufacturer's instructions. Images were obtained using an Axiovert 200 M microscope (Zeiss) and analyzed with ImageJ software in order to determine the fraction of EdU positive nuclei. Images of 6 random fields were analyzed per treatment and experiment.

2.8. Microfluidic chemotaxis assay

Migration in response to a stabile gradient of factors was assessed as previously described [26,27]. In short, cells were seeded onto a gelatin coated 35 mm tissue culture dish (BD Falcon), allowed to attach and starved over night after which the microfluidic chamber was applied on top and a gradient generated using indicated factors in serum free medium. Factors gradients used were PDGF-BB (Peprotech) 0–20 ng/ml, FnE, FgnE and FnDD (Hyphen biomed) 0–2 nM over a distance of 500 µm with a flow rate of 1.5 µl/min. Cell movement was recorded using an Axiovision 200 M microscope (Zeiss) for 4 h and tracked using Axiovision software (Zeiss). Cells were kept at 37 ˚C with 5% CO_2 in a humid atmosphere during the experiments. When inhibitors were used, cells were pre-incubated 1 h before assembly of the migration chamber, followed by presence of the inhibitor in the entire chamber for the entire duration of the experiment. For siRNA treated cells the assay was initiated 46–50 h post-nucleofection. Data is presented as chemotaxis distance, measuring movement towards the high end of the gradient, and net distance, measuring the average distance of migration between start- and end points of the individual cells.

2.9. SPR biosensor analyses

SPR biosensor measurements were performed at 25 ˚C using a Biacore S51 instrument (Cytiva, Uppsala, Sweden). FnE and FnDD were immobilized with standard amine coupling procedure to a CM5 chip with sodium acetate at pH 4 as the immobilization buffer, to approximately 950 response units (RU) FnE and 1251 or 5226 RU for FnDD. PBS buffer at pH 7.4 with 0.005% P20 was used as running buffer, and integrin $\alpha_V\beta_3$ was run as analyte in four different concentrations using a flow rate of 30 µL/min. The surface was regenerated with glycine-HCl at pH 2 between each cycle for the interaction with FnE and integrin $\alpha_V\beta_3$. The sensorgrams were corrected for buffer bulk effects and unspecific binding of the samples to the chip matrix by blank and reference surface subtraction (subtraction of inactivated and deactivated flow cell channel). The data were analyzed using Biacore T200 evaluation software version 1.0. The sensorgrams of the interaction between FnE and integrin $\alpha_V\beta_3$ were fitted to several binding models, including 1:1 (Langmuir) binding model, two-state reaction (conformational change) model, bivalent analyte and heterogeneous ligand model. The association and dissociation kinetic rate constants (k_a, and k_d, respectively) and the dissociation constant (K_D), or equivalent, were estimated for each model.

2.10. Mini-osmotic pump implantation

10-week-old, female C57Bl/6 (Crl) mice were obtained from Scanbur (Denmark) and randomly divided in 2 experimental groups; FnE (n = 6) and saline control (n = 6). Mice were housed in standard conditions with normal dark-light cycle. This method was approved by the ethical committee for animal experimentation in Uppsala (C45/13) and conform to the Animal Research: Reporting of *In Vivo* Experiments guidelines developed by the National Centre for the Replacement, Refinement and Reduction of Animals in Research. Animals were acclimated to their environment for 1 week and given *ad libitum* access to water and food. Mini-osmotic pumps (Alzet 1002, 0,25 µl/h) containing FnE (200 ng/µl with 0,1% BSA in saline) or controls (0,1% BSA in saline) were implanted subcutaneously in mice anesthetized with isoflurane (Forene). Post-operative analgesia (Temgesic) was provided daily for 3 days. After exposure to 50 ng/h FnE or saline (control) for 2 weeks, skin biopsies were collected around the pump using 4 mm biopsy punches. Tissues were fixed in 4% PFA and dehydrated and embedded in paraffin before being sectioned in 5 µm sections. Sections were de-parafinized and rehydrated before being blocked in 10% hydrogen peroxide and 1% BSA in PBS. Immunohistochemical staining for α-SMA (clone 1A4, Sigma) was performed using an HRP-coupled anti-mouse antibody with DAB as a substrate. Antibody incubation times were 1 h at room temperature. The samples were washed in TBS-T (0.1% Triton-X100) 3 × 10 minutes after primary and secondary antibody incubations. A standard hematoxylin and eosin staining was done to assess general morphology. Collagen was stained using Sirius Red and Masson trichrome staining. Sirius Red staining was performed after serial deparaffinizing and dehydration steps, by incubation of 45 min in 1% pico-sirius red (Sigma-Aldrich) in a saturated aqueous

solution of picric acid (Sigma-Aldrich). Masson trichrome was stained using a commercial staining kit (HT15, Sigma-Aldrich) following manufacturer's guidelines. Quantifications were performed blindly with ImageJ software by conversion to binary images after color deconvolution to separate DAB, Sirius red or Masson trichrome staining, as previously described [28].

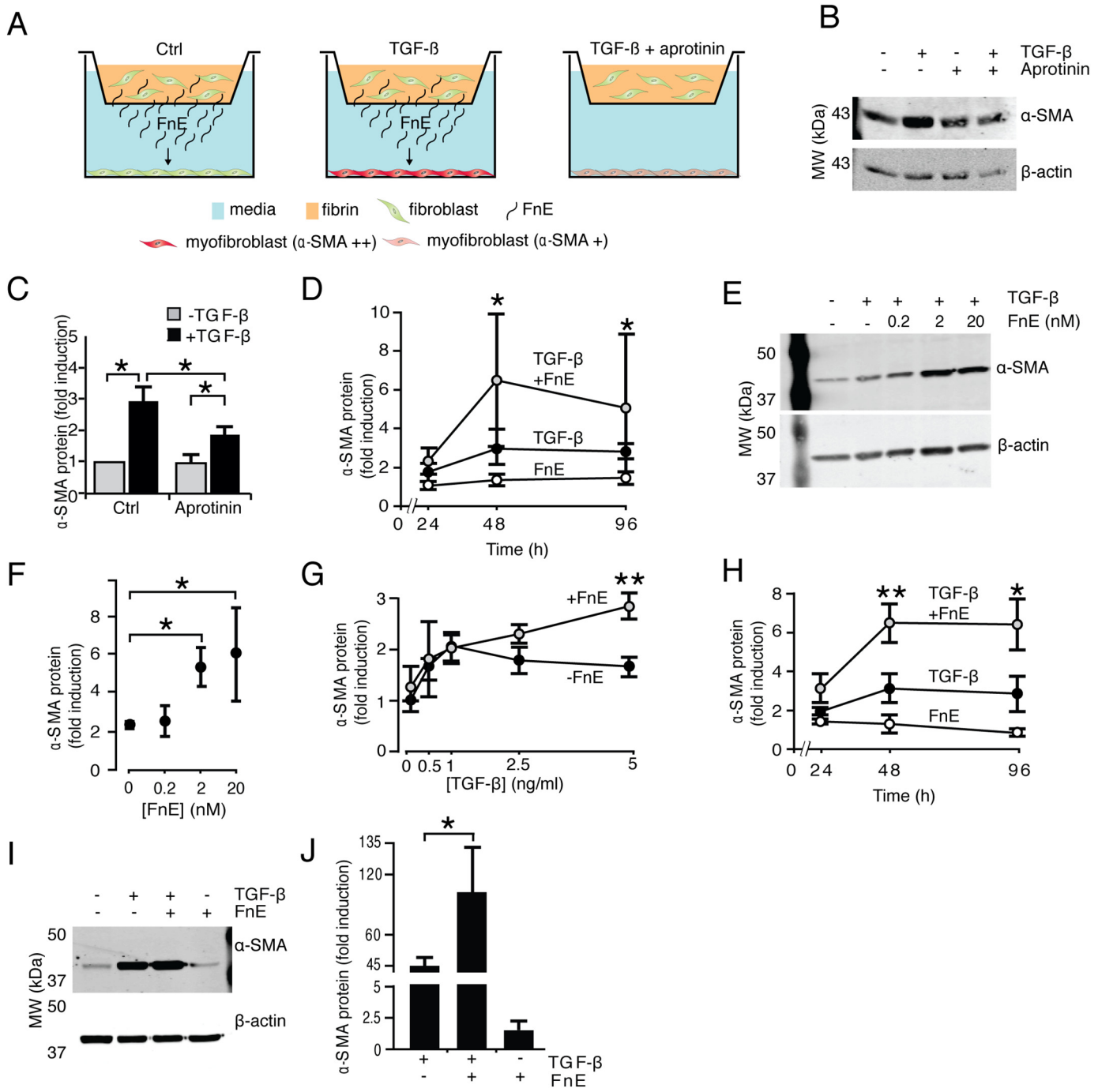

Fig. 1. FnE synergistically enhance TGF-β-induced α-SMA protein expression in a time- and dose-dependent manner. (A) Human HFL1 fibroblasts were grown in transwell inserts in a fibrin gel, as well as on the bottom of the well, and treated as indicated. (B) Representative western blot for α-SMA obtained from cells growing on the bottom of the well 48 h after stimulation with or without TGF-β (5 ng/ml). (C) Quantification of the results in B normalized to β-actin and expressed as fold increase compared to unstimulated control ($n = 3$). (D) HFL1 fibroblasts were starved and cultured in the presence of either TGF-β (5 ng/ml), or FnE (2 nM), or both factors for the indicated periods of time. α-SMA levels were determined by western blotting and normalized to β-actin and expressed as fold increase compared to control cells ($n = 4$). (E) Representative western blot showing the dose-dependent potentiation of TGF-β-induced α-SMA expression by FnE and (F) quantification of the results normalized to β-actin and expressed as fold increase compared to controls (n = 3). (G) α-SMA protein levels in HFL1 cells cultured with or without FnE (2 nM) and increasing concentrations of TGF-β (n = 3). (H) α-SMA protein levels in human BJ hTERT fibroblasts treated either with TGF-β or with FnE, or a combination of both (n = 3). (I) Representative western blot showing α-SMA protein expression in rat NRK-49F fibroblasts cells after a 48 h stimulation with TGF-β (5 ng/ml), FnE (2 nM) or a combination of both and (J) quantification of the results normalized β-actin and expressed as fold increase compared to controls ($n = 5$). * $p < .05$, ** $p < 0{,}01$. Error bars represent standard deviation, n refers to number of biological replicates per group.

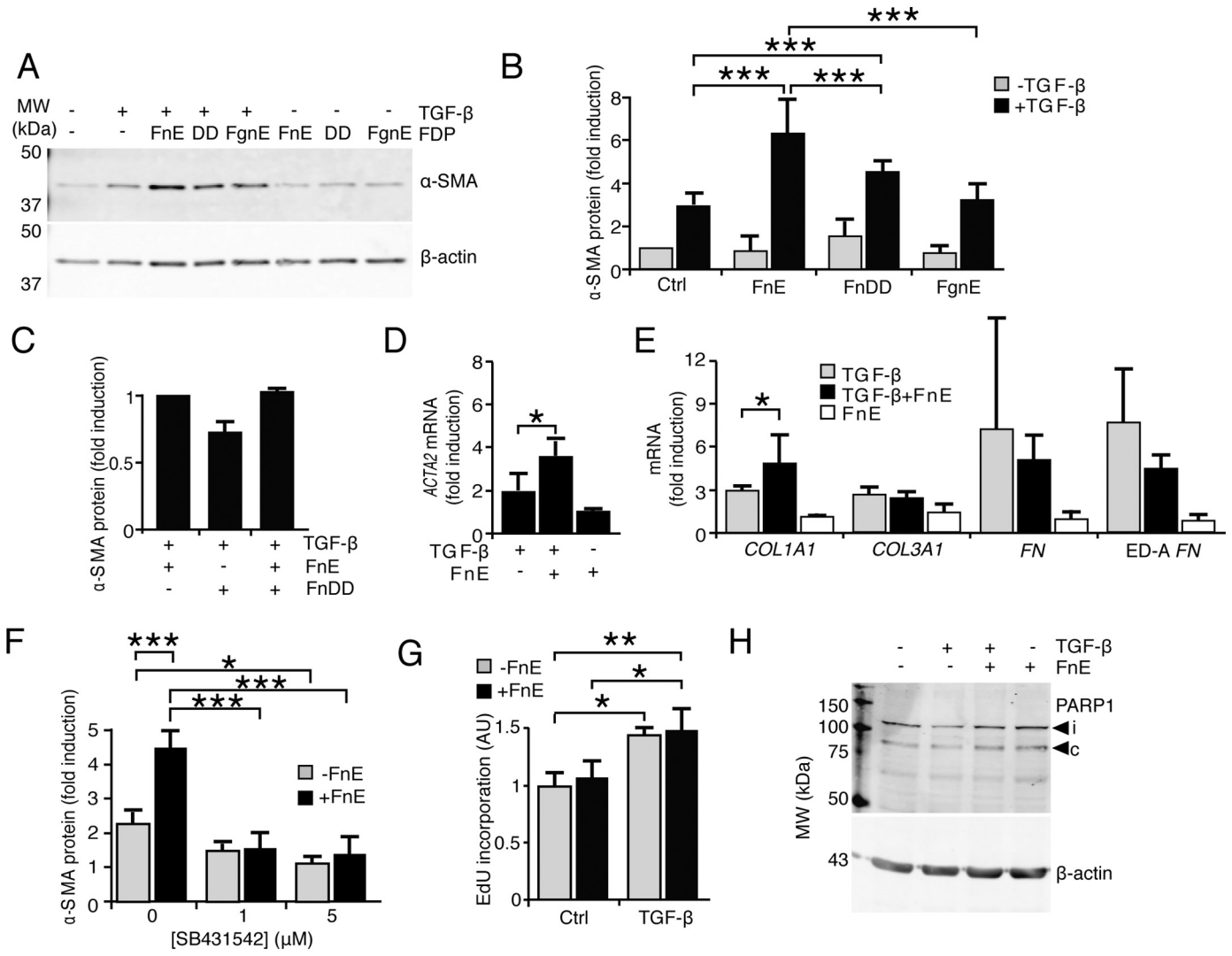

Fig. 2. FnE and FnDD but not FgnE enhance TGF-β-induced myofibroblast activation. (A) Representative western blot and (B) quantification of α-SMA protein levels in HFL1 cells cultured for 48 h with TGF-β (5 ng/ml) alone or in combination with different FDPs (2 nM) ($n = 9$). Values in (B) are normalized to β-actin and expressed as fold increase compared to untreated control cells cultured in starvation medium. (C) α-SMA protein expression in HFL1 cells after a 48 h stimulation with TGF-β in combination with FnE and/or FnDD. (D) Relative α-SMA (*ACTA2*) mRNA expression and (E) other major matrix component transcripts in HFL1 cells after a 48 h treatment with the indicated factors (TGF-β, 5 ng/ml; FnE, 2 nM); collagen Iα1 (*COL1A1*), collagen IIIα1 (*COL3A1*), fibronectin (*FN*) and extra domain A containing fibronectin (EDA *FN*) ($n = 4$). (F) TGF-β (5 ng/ml) and TGF-β + FnE (2 nM) induced α-SMA protein expression in HFL1 cells is inhibited by a 48 h treatment using the TGF-β receptor kinase inhibitor SB431542 ($n = 3$). (G) Proliferation in response to TGF-β (5 ng/ml), FnE (2 nM) or a combination of both for 48 h, expressed as the fraction of EdU positive nuclei in treated cells compared to unstimulated control cells (n = 3). (H) Western blot showing the levels of PARP-1 in HFL1 cells treated or not with TGF-β and FnE; molecular species corresponding to the cleaved (c) and intact (i) forms are indicated by arrows. * $p < .05$,*** $p < 0{,}001$. Error bars represent standard deviation, n refers to number of biological replicates per group.

2.11. Statistics

Statistical analyses of cell cultured derived data was performed using two-sided one sample *t*-test, student's t-test or analysis of variance (ANOVA) followed by tukey-correction *post hoc* test, animal data was analyzed using the two-sided Mann-Whitney *U* test. All statistical analyses were carried out in the GraphPad Prism 5 software (GraphPad software). *P*-values < .05 were considered statistically significant. *In vitro* experiments were done in at least 3 individual biological replicates, *in vivo* experiments were performed on 6 independent animals. Values are presented as mean ± standard deviation, mouse data are additionally presented by individual dots.

2.12. Study approval

The use of the mouse model and methods have been approved by the Uppsala Animal Experiment Ethics Board.

3. Results

3.1. FnE potentiates expression of α-SMA induced by TGF-β

To study if degradation products released from fibrin gels could affect α-SMA expression in fibroblasts, a transwell assay was employed with fibroblasts embedded in a fibrin gel in the insert and effects on fibroblasts at the bottom of the well examined (Fig. 1A). First, TGF-β was shown to induce α-SMA expression in human fetal lung fibroblasts (HFL1) and the expression of α-SMA could be decreased by the addition of serine protease inhibitor aprotinin (Fig. 1B, C). This experiment suggested that FDPs released from the gel by cell-derived proteases stimulated TGF-β –induced α-SMA expression in an additive or synergistic manner. This possibility was further investigated using

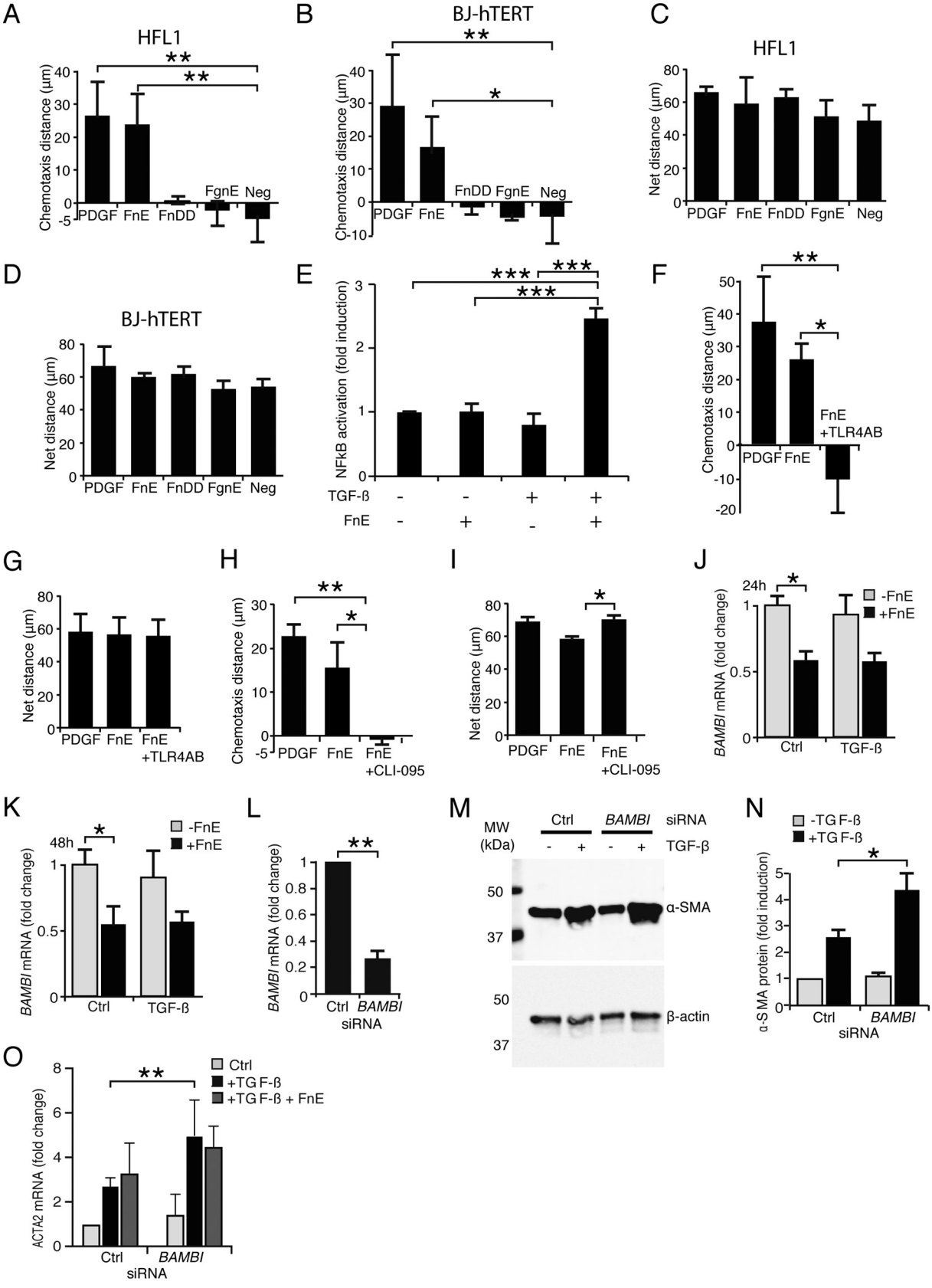

(caption on next page)

Fig. 3. FnE-induced fibroblast chemotaxis is dependent on TLR4 and on interactions with $\alpha_V\beta_3$ integrins. (A) HFL-1 (n = 3) and (B) BJ-hTERT (n = 4) fibroblasts were exposed to stabile gradients of either PDGF-BB (positive control) or the different FDPs using a microfluidic chemotaxis assay to study effects on cell migration. Of the FDPs, only a gradient of FnE elicited a chemotactic response. The net distance migrated by (C) HFL-1 (n = 3) and (D) BJ-hTERT (n = 4) fibroblasts irrespective of directionality was also scored. (E) NFkB activation in HFL1 cells 48 h after stimulation with TGF-β (5 ng/ml), FnE (2 nM) or a combination of both (n = 3). (F) Chemotaxis and (G) net distance migrated by HFL1 cells in the presence of the TLR4-blocking antibody (n = 4). (H) Chemotaxis and (I) net distance migrated by HFL1 cells in the presence of the TLR4 inhibitor CLI-095 (n = 4). *BAMBI* mRNA levels in HFL1 cells 24 h (J) and 48 h (K) after treatment with TGF-β (5 ng/ml) and/or FnE (2 nM) (n = 4). (L) Suppression of *BAMBI* mRNA levels using siRNA (n = 3). (M, N) Representative western blot and corresponding quantifications of the α-SMA protein levels in siRNA-treated cells with and without TGF-β (5 ng/ml) stimulation (n = 3). Relative α-SMA (*ACTA2*) mRNA expression in siRNA-treated cells with and without TGF-β and FnE (n = 4). * $p < .05$,** $p < 0{,}01$. Error bars represent standard deviation, n refers to number of biological replicates per group.

purified FnE, which when added to HFL1 cells potentiated TGF-β-induced α-SMA expression by around two-fold in a dose-dependent manner (Fig. 1D, E, F). Notably, FnE did not alter the basal α-SMA expression levels when added alone (Fig. 1D). No significant differences were seen in intracellular and secreted levels of TIMP1, a metalloproteinase inhibitor, suggesting the effect was not due to increased breakdown of the extracellular matrix (Supplementary Fig. 1). The effect of FnE reached a maximum at 2 nM after 48 h (Fig. 1H). Addition of a fixed concentration of FnE (2 nM) together with increasing concentrations of TGF-β revealed that the synergistic effect was present at 5 ng/ml TGF-β, but not at lower concentrations (Fig. 1G). FnE was also shown to potentiate TGF-β-induced α-SMA expression in immortalized human foreskin fibroblasts (BJ hTERT, Fig. 1H) and rat kidney fibroblasts (NRK−49F, Fig. 1I, J), suggesting that the response to FnE is a basic feature of fibroblasts.

In order to elucidate if other FDPs than FnE could impact α-SMA expression, we investigated the effects of adding the E fragment from non-cross-linked fibrinogen (FgnE) or D-dimer (FnDD) from cross-linked fibrin to HFL1 cells. At equimolar concentrations, FgnE had no effect while FnDD potentiated TGF-β induced α-SMA expression, although to a lesser extent than FnE (Fig. 2A, B). Neither FnE nor FgnE nor FnDD altered the basal α-SMA expression levels. Further, FnDD could not enhance α-SMA expression when added together with FnE (Fig. 2C).

Collagen I, collagen III, fibronectin and extra domain A fibronectin (ED-A FN) are, in addition to α-SMA, proteins that are associated with myofibroblast activation. Besides α-SMA mRNA (*ACTA2*), FnE also increased TGF-β-stimulated Collagen Iα1 mRNA (*COL1A1*) but not Collagen III α1 (*COL3A1*), fibronectin (*FN*) or ED-A containing fibronectin (*ED-A FN*) in HFL1 cells (Fig. 2 D, E). Inhibition of TGF-β receptor signaling by the low molecular inhibitor SB431542 blocked both TGF-β-induced as well as FnE-mediated potentiation of α-SMA expression in HFL1 cells (Fig. 2F), demonstrating that TGF-β signaling is critical in order for FnE to exert its effect on α-SMA potentiation.

3.2. FnE does not influence cell proliferation or induce apoptosis

It has been reported that FnE stimulates endothelial cell proliferation [23] and induces apoptosis [29]. Here, TGF-β caused a slight increase in proliferation of HFL1 cells but FnE alone, or in combination with TGF-β, had no effect (Fig. 2G). Treatment of HFL1 cells with FnE did not increase apoptosis as measured by increased cleavage of the DNA-repair enzyme PARP-1, which is commonly used as an indication of apoptosis [30] (Fig. 2H).

3.3. FnE is chemotactic for fibroblasts

FnE has previously been reported to induce migration of endothelial and vascular smooth muscle cells. We therefore investigated the chemotactic effects of FnE on fibroblasts. A microfluidic cell migration chamber [26,27] was used to analyze the effects of stable gradients of FDPs on chemotaxis and chemokinesis of individual cells using time-lapse microscopy. FnE was the only FDP that had a chemotactic effect (Fig. 3A, B) similar to that of the positive control PDGF-BB. The net migration distance (irrespective of direction) was similar for all FDPs investigated (Fig. 3C, D) indicating that none of them induced a chemokinetic response.

3.4. FnE-mediated chemotaxis is dependent on toll like receptor 4 and BAMBI

Toll-like receptor 4 (TLR4) has been reported to bind fibrinogen [31] and thereby to regulate proliferation of fibroblasts [32], which makes TLR4 a candidate receptor for FnE. The combination of TGF-β and FnE lead to a significant activation of NFkB, which could mean that TLR4 is involved in FnE's potentiation of TGF-β (Fig. 3E). Treatment of HFL1 fibroblasts with a specific blocking antibody against TLR4 (Fig. 3F, G) and the TLR4 inhibitor CLI-095 (also known as TAK-242) (Fig. 3H, I) [33] inhibited the chemotactic effect of FnE (Fig. 3H, I). This supported our hypothesis that TLR4 is a candidate receptor for FnE. Bacterial lipopolysaccharide (LPS) has been shown to enhance TGF-β signaling by TLR4 mediated down-regulation of the TGF-β pseudo-receptor BAMBI [34]. In agreement, FnE treatment of HFL1 cells caused a 50% reduction in *BAMBI* mRNA levels already after 24 h (Fig. 3J), which persisted for at least 48 h (Fig. 3K). Reduction of BAMBI levels with siRNA (Fig. 3L) mimicked the effect of FnE with potentiation of TGF-β induced α-SMA expression without addition of FnE (Fig. 3M, N). Combining BAMBI knockdown with FnE stimulation did not induce a synergistic effect on α-SMA expression (Fig. 3O). No significant differences were seen in intracellular and extracellular levels of TGF-β after addition of FnE (Supplementary Fig. 2).

3.5. FnE-mediated chemotaxis and α-SMA induction depend on β3 integrins

Both fibrinogen and fibrin contain several tripeptide arginine-glycine-aspartate (RGD) sequences, making them potential binding partners for RGD-binding integrins. In order to investigate if FnE interacts with integrins with a biologically relevant mechanism and affinity, direct binding experiments were performed using surface plasmon resonance (SPR) biosensor technology. Thus, FnE was immobilized onto a sensor chip and soluble recombinant human $\alpha_V\beta_3$-integrin injected as an analyte over the surface of the chip [20]. $\alpha_V\beta_3$-integrin displayed a concentration-dependent interaction with FnE, forming a stable complex (Fig. 4A). This was not observed for FnDD (Fig. 4B). The binding curves were not well described by a simple 1:1 binding model, suggesting that the interaction was more complex (Fig. 4C). The slow dissociation rates indicate a strong interaction with a dissociation constant (K_D) in the low in nM range (2–20 nM dependent on interaction model). To further investigate the potential importance of the RGD element in FnE a cyclic-RGD peptide EMD 66203 (cRGD) was used, which competes for the binding to RGD binding integrins. cRGD treatment eliminated the synergistic effect of FnE on TGF-β-induced α-SMA expression in HFL1 cells, but did not affect the response to TGF-β alone (Fig. 4D, E). In contrast, treatment with cRGD increased both chemotaxis as well as the total distance migrated of HFL1 cells in response to PDGF-BB and FnE gradients (Fig. 4F, G). Notably, however, the ratio between chemotaxis and the total distance migrated remained similar compared to previous results, indicated by dashed grey lines.

The cRGD peptide targets the $\alpha_V\beta_3$–integrin complex as well as the $\alpha_V\beta_5$-integrin complex [35]. In order to elucidate if both of these

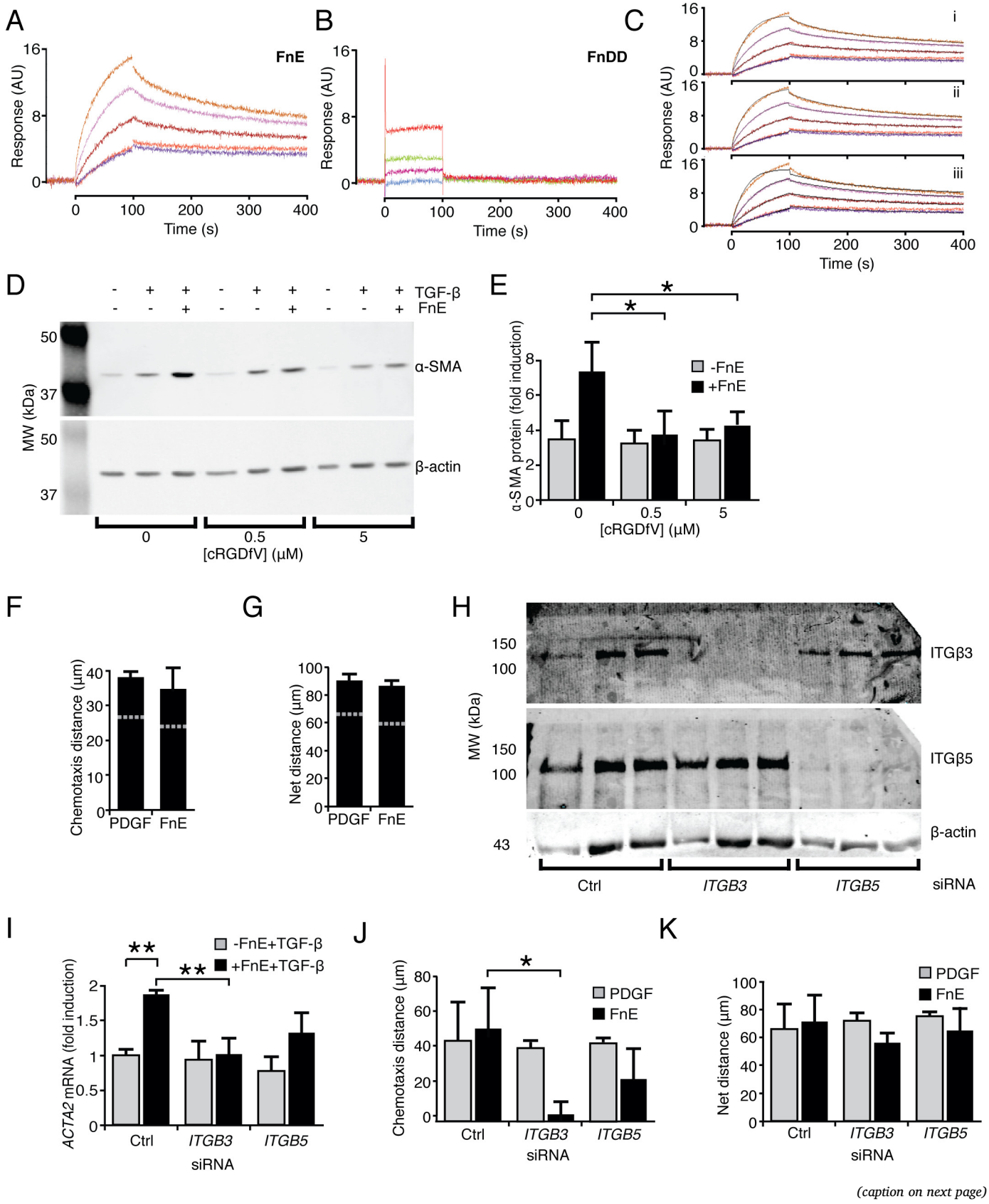

(caption on next page)

complexes are involved in mediating the effects of FnE we performed siRNA knockdown experiments targeting either integrin β3 or β5 in HFL1 cells. Robust reductions in integrin β3 and β5 protein levels as a result of siRNA treatment were confirmed by Western blotting (Fig. 4H). siRNA-mediated suppression of integrin β3, but not β5, abolished the potentiating effect of FnE on TGF-β-induced α-SMA mRNA expression (Fig. 4I). A reduction of the integrin β3 levels also diminished the chemotaxis towards FnE whereas a reduction of the

Fig. 4. FnE-mediated potentiation of α-SMA expression is dependent on interactions with $\alpha_V\beta_3$ integrins. Interactions between soluble recombinant $\alpha_V\beta_3$ (5–50 nM) and immobilized FnE (A) or FnDD (B) were determined by SPR (n = 5). Immobilization was at 952 RU and 1251 RU respectively. (C) SPR sensorgrams of the interaction between FnE and integrin $\alpha_V\beta_3$ fitted to a bivalent analyte model (i), a heterogeneous ligand model (ii) or to the 1:1 two state interaction model (iii). (D) Representative western blot and (E) quantification of α-SMA protein levels of HFL1 fibroblasts in the presence of the cyclic-RGD peptide EMD 66203 in combination with TGF-β (5 ng/ml) and/or FnE (2 nM) (n = 4). α-SMA was normalized against β-actin and expressed as compared to vehicle (DMSO) treated controls. (F) Chemotaxis and (G) net migration of HFL1 cells in presence of 5 μM cyclic-RGD peptide (n = 4). Dashed grey lines indicate mean values for cells without addition of cyclic- RGD. (H) Integrin β3 and β5 protein levels in HFL1 cells after transfection with siRNA selectively targeting these integrins, as indicated. (I) α-SMA (*ACTA2*) mRNA levels of siRNA transfected cells stimulated with TGF-β (5 ng/ml) with or without addition of FnE (2 nM) for 48 h (n = 3). (J) Chemotaxis and (K) net migration of HFL1 cells treated with siRNA to suppress integrin β3 or β5 in response to a PDGF-BB (0–20 ng/ml) or FnE (0–2 nM) gradients (n = 4). * $p < .05$,** $p < 0{,}01$. Error bars represent standard deviation, n refers to number of biological replicates per group.

integrin β5 levels had no significant effect on FnE-induced chemotaxis (Fig. 4J). Notably, PDGF-BB-induced chemotaxis as well as general cell motility in any condition was not affected by suppression of β3 or β5 integrins (Fig. 4J, K).

3.6. Profibrotic effects of FnE in vivo

In order to validate these *in vitro* results, we used an *in vivo* mouse model where profibrotic effects are analyzed after continuous subcutaneous infusion of FnE by mini-osmotic pumps. A single pump loaded with FnE or saline (control) was implanted subcutaneously on the back of C57/BL6 mice and kept in place for 2 weeks. Immunohistochemical analysis of sections of skin taken from the area in proximity to the infusion site revealed that FnE-treated mice displayed an increased number of α-SMA-positive myofibroblasts in the hypodermis (Fig. 5A, B, C). This also led to an increased deposition of collagen, as measured on Sirius red (Fig. 5 D, E and F) and Masson Trichrome (Firugre 5 G, H I) staining.

4. Discussion

Deposition of a fibrin-rich matrix in the interstitium is an integral part of tissue repair and fibrin deposits are in addition found in association with tumors [11,36], rheumatoid arthritis [37], inflammatory diseases and fibrotic conditions [3,18–20,38] where fibrin has been proposed to promote disease development. During tissue injury, circulating fibrinogen will generate a dense network of cross-linked fibrin upon activation of the coagulation cascade. This network provides a scaffold that directly interacts with cells to create a hemostatic plug. The fibrin scaffold also provides a provisional matrix for wound repair and tissue regeneration. The continuous degradation of fibrin generates the FDPs, fibrin fragment E and D-dimer. In this study we provide evidence that low nanomolar concentrations of FnE stimulates fibroblast migration comparable to that of PDGF-BB, which is a strong chemoattractant [39] and potentiates TGF-β induced myofibroblast formation.

FnE, in contrast to polymerized fibrin, is freely diffusible and we suggest that FnE released from polymerized fibrin by proteolysis forms a concentration gradient that recruits fibroblasts to the injured tissue as demonstrated by our live-cell tracking experiments. As the fibroblast move closer to the fibrin clot they become increasingly activated by higher levels of FnE and other growth factors and cytokines. The initial recruitment of fibroblasts is likely also dependent on local and acute release of PDGF-BB from platelets, while FnE may act to continuously recruit fibroblasts as long as there is degradation of fibrin deposits.

One factor in particular that fibroblasts encounter as they migrate into the wounded area is TGF-β. This potent cytokine is produced by neutrophils and macrophages present in the wound, as well as by keratinocytes and fibroblasts. As demonstrated here, FnE is capable of enhancing TGF-β-induced α-SMA expression and collagen I production. Notably, as FnE does not induce the transition towards a myofibroblast phenotype by itself, only fibroblasts that are migrating into TGF-β-rich areas of the wound would become fully activated into myofibroblasts. Accordingly, when mice were implanted with mini-osmotic pumps that continuously released FnE, a significant increase of α-SMA positive cells was observed near the implantation site, which indeed is a wounded area due to the surgical procedure that was needed to implant the pumps. Fibroblast activation is a multi-step process, which initially results in an increase of cell migration and proliferation, without increasing extracellular matrix production. In later stages of fibroblast activation, migration and proliferation decreases, while the production of ECM expands. In our study, we see an increase in α-SMA and chemotaxis in response to FnE and TGF-β, as well as increased *COL1A1*. However, we did not see an increase in *COL3A1* or *fibronectin*. This issue may be related to the cells used, as we have used commercial cell lines (HFL1 and BJ), which were maintained and passaged. It is likely that conversion to myofibroblasts was already underway prior to the stimulation with growth factors and this is supported by the clear expression of α-SMA even in non-stimulated cells. Thus, the cells used may be a heterogeneous population of variously activated fibroblasts and myofibroblasts.

Interestingly, FnE down-regulated BAMBI, which is a pseudoreceptor that interacts with TGF-β and BMP type II receptors [40] to form a non-signaling receptor complex that negatively modulates TGF-β responses. Reduced BAMBI expression potentiated TGF-β-induced responses. These results are in line with a previous study where TGF-β-induced α-SMA and collagen I expression was enhanced by down-regulation of BAMBI [41].

The Toll-like receptors have until recently been considered to mediate only innate immune responses but have lately been shown to bind endogenous ligands such as hyaluronan [42], HMGB1 [43] and fibrinogen [31]. Although TLR4 is mainly expressed by immune cells as part of the innate immune system, TLR4 activation has also been shown to occur in non-immune cells within injured tissue micro-environments, such as renal fibrosis [44] and scleroderma [45,46]. Our data now suggests that TLR4 modulates FnE-stimulated fibroblast migration. Fibroblast chemotaxis in response to FnE also requires integrin β_3 as determined here by siRNA knockdown experiments. $\alpha_V\beta_3$ integrin was also found to bind directly to FnE, forming a very stable complex (Fig. 4). Studies have shown that integrins can function as ligand-binding co-receptors that induce TLR activation and downstream signaling in fibroblasts [47]. In agreement with this, the synergistic effect of FnE on TGF-β induced α-SMA expression through was dependent on integrin $\alpha_V\beta_3$ as shown by using the cRGDfV peptide and by knockdown of β_3 with siRNA. The finding that inhibition of $\alpha_V\beta_3$ and $\alpha_V\beta_5$ using cRGDfV did not reduce the FnE induced chemotaxis may be due to that at any given time there may be enough free $\alpha_V\beta_3$ to distinguish between the high and low concentration end of the FnE gradient. In our study, FnE or TGF-β alone did not induce a significant activation of NFkB. There have been several reports suggesting a cross-talk between NF-kB and TGF-β pathways, which could explain the synergistic effect of TGF-β and FnE in regards to NF-kB activation [48,49]. A graphical overview of our proposed model is provided in Fig. 6.

Subcutaneous infusion of FnE into mice induced a profibrotic response with increased number of α-SMA positive myofibroblasts in the hypodermis. These results suggest a role for FnE in fibrotic conditions in agreement with the proposed functions of fibrin, fibrinogen and FDPs in wound healing and inflammation. In wound healing, FnE might promote recruitment and activation of myofibroblasts and enhance the formation of granulation tissue. FnE could also contribute to

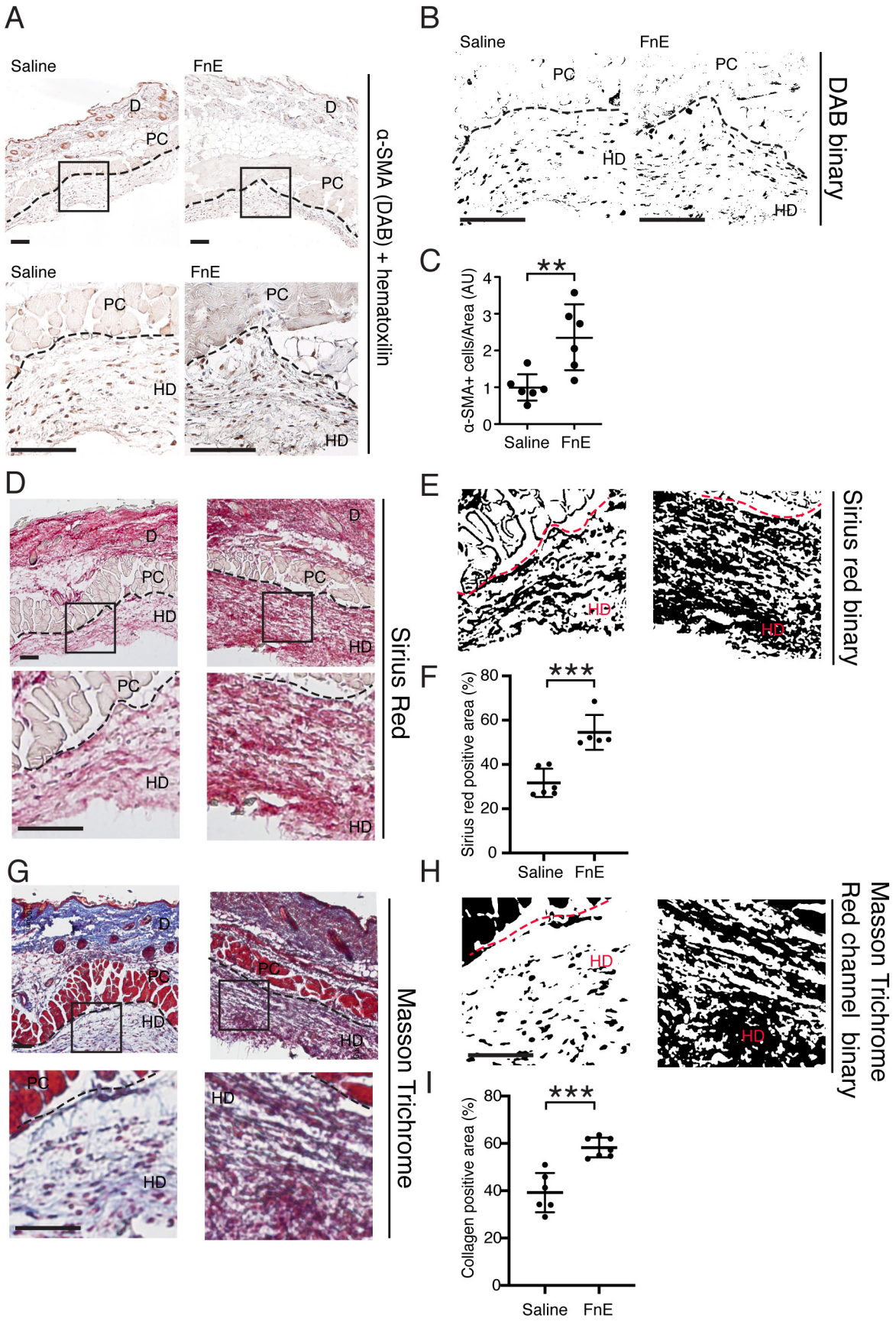

(caption on next page)

Fig. 5. FnE-infusion results in increased numbers of α-SMA positive cells in the hypodermis of mice *in vivo*. Mini-osmotic pumps containing either saline (control) or FnE (20 μg) was implanted subcutaneously in C57Bl/6 mice and left in place for 2 weeks. (A) α-SMA-positive cells in mouse hypodermis (HD) were identified by immunohistological staining near the infusion site. D, dermis; PC, panniculus carnosus; Color de-convolution and conversion to binary images (B) was performed to enable quantification of α-SMA-positive cells. (C) α-SMA+ cells/area HD was quantified. (D) Collagen fibers were identified by Sirius red staining and (G) Masson trichrome staining. Color de-convolution and conversion to binary images (E) and (H) was performed to enable quantification of percentage of collagen in the hypodermis on Sirius Red (F) and Masson Trichrome (I). Scale bar 100 μm, ** $p < 0{,}01$, *** $p < 0{,}001$. Individual mice are represented by dots. Error bars represent standard deviation ($n = 6$ per group). (For interpretation of the references to color in this figure legend, the reader is referred to the web version of this article.)

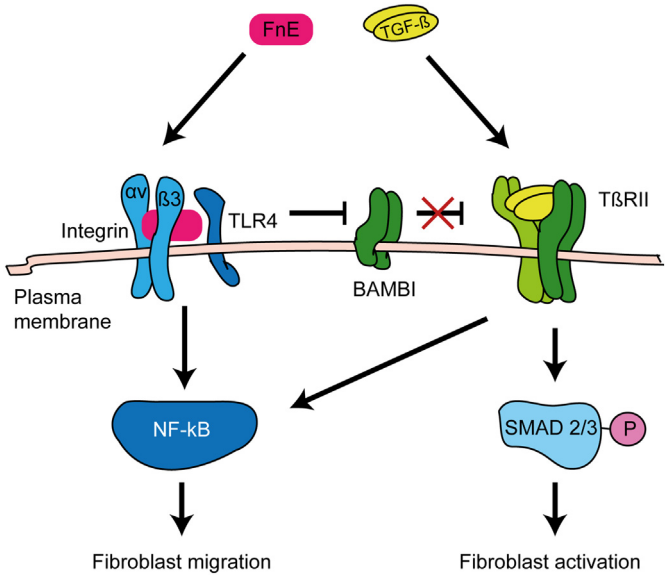

Fig. 6. Graphical overview depicting the suggested mechanism on how FnE influences fibroblast migration and activation. We show that FnE forms a stable complex with $\alpha_V\beta_3$ integrins, which then affects both TLR4 signaling and inhibits the expression of BAMBI. BAMBI is a pseudoreceptor that interacts with TGF-β and BMP type II receptors to form a non-signaling receptor complex that negatively modulates TGF-β responses, including the activation of fibroblasts. Therefore, the FnE-induced down-regulation of BAMBI potentiates the effect of TGF-β on fibroblast activation. We also show that TLR4 modulates FnE-stimulated fibroblast migration, which requires integrin β_3 as determined here by siRNA knockdown experiments.

revascularization through looping angiogenesis where myofibroblast mediated contraction of the provisional matrix creates biomechanical forces that mediate and direct neovascularization [50]. In addition, fibrin antibodies have also been shown to directly inhibit angiogenesis, thus further indicating a role for FnE in neovascularization [51], which is an essential aspect in wound healing, but also contributes to progression and metastasis of solid tumors. The release of FnE from fibrin deposits in wounds and tumors would form stable gradients to direct recruitment of fibroblasts as long as fibrin deposits are present. Tumors have historically been called “a wound that does not heal” [52]. Given the deposition of fibrin and the disruption of coagulation pathways found within many tumors, it is possible that FnE may be involved in tumor progression by recruiting cancer-associated fibroblasts [53]. These fibroblasts are known to promote tumorigenesis, by initiating the remodeling of the extracellular matrix and by secreting cytokines [11]. In support, there are indications that cancer patients treated with anticoagulants have an increased survival, which is not solely due to a decreased incidence of thromboembolic events [54–56]. The findings in animal models that an antibody against FnE inhibits tumor growth [57] and that metastasis is reduced in fibrinogen deficient animals [58] further supports such a concept.

Accumulating evidence suggests a role for fibrinogen, fibrin and FDPs in fibrotic disease. Fibrinogen-deficient mice are protected from kidney fibrosis in a model of unilateral urethral obstruction with reduced number of fibroblasts, lower levels of α-SMA expression and less collagen I production [32]. Further evidence for a role in fibrosis is provided by the finding that injection of fibrin into the tunica albuginea in mice induces fibrotic response similar to Peyronie's disease in humans [59]. Fibrin deposition is also one of the most conspicuous and consistent features of both human rheumathoid arthritis and experimental animal models of arthritic disease [60].

5. Conclusions

The current study shows that FnE at low nanomolar concentrations is a potent inducer of fibroblast chemotaxis, enhances myofibroblast activation, and is profibrotic *in vivo*. These results further expand the role of fibrin beyond hemostasis, and may have implications for the understanding of the pathophysiology of wound healing, fibrosis and tumor growth.

Supplementary data to this article can be found online at https://doi.org/10.1016/j.cellsig.2020.109661.

Declaration of Competing Interest

The authors declare that there is no conflict of interest.

Acknowledgements

This work was supported by grants from the Swedish Research Council (2010-3968 and K2011-66X-15348-07-3), the Swedish Cancer Society (CAN2017/518, CAN2013/1273 and CAN 2011/465), Swedish society for medical research (SSMF, S17-0092), the Swedish Childhood Cancer Foundation (PROJ09/114), the Wenner-gren foundation and the Lion Cancer Research Foundation, the Olga Jönssons Foundation and Lennanders Foundation for the advancement of medical and scientific research.

References

[1] A. Vranic, I. Pruner, M. Veselinovic, N. Soutari, A. Petkovic, V. Jakovljevic, A. Antovic, Assessment of hemostatic disturbances in women with established rheumatoid arthritis, Clin. Rheumatol. 38 (11) (2019) 3005–3014.
[2] Y. Kanno, The role of fibrinolytic regulators in vascular dysfunction of systemic sclerosis, Int. J. Mol. Sci. 20 (3) (2019).
[3] W. Potze, R.J. Porte, T. Lisman, Management of coagulation abnormalities in liver disease, Expert Review of Gastroenterology & Hepatology 9 (1) (2015) 103–114.
[4] Y. Wang, O.B. O, S. Zhang, L. Luo, E. Norstrom, H. Thorlacius, Dynamic changes in thrombin generation in abdominal sepsis in mice, Shock 42 (4) (2014) 343–349.
[5] K. Ntelis, D. Bogdanos, T. Dimitroulas, L. Sakkas, D. Daoussis, Platelets in systemic sclerosis: the missing link connecting vasculopathy, autoimmunity, and fibrosis? Curr. Rheumatol. Rep. 21 (5) (2019) 15.
[6] J. Devereaux, K. Nurgali, D. Kiatos, S. Sakkal, V. Apostolopoulos, Effects of platelet-rich plasma and platelet-poor plasma on human dermal fibroblasts, Maturitas 117 (2018) 34–44.
[7] G. Gabbiani, The myofibroblast in wound healing and fibrocontractive diseases, J. Pathol. 200 (4) (2003) 500–503.
[8] G. Gabbiani, B.J. Hirschel, G.B. Ryan, P.R. Statkov, G. Majno, Granulation tissue as a contractile organ. A study of structure and function, J. Exp. Med. 135 (4) (1972) 719–734.
[9] F. Heindryckx, F. Binet, M. Ponticos, K. Rombouts, J. Lau, J. Kreuger, P. Gerwins, Endoplasmic reticulum stress enhances fibrosis through IRE1alpha-mediated degradation of miR-150 and XBP-1 splicing, EMBO Molecular Medicine 8 (7) (2016) 729–744.
[10] F. Heindryckx, J.P. Li, Role of proteoglycans in neuro-inflammation and central nervous system fibrosis, Matrix Biol. 68–69 (2018) 589–601.
[11] F. Heindryckx, P. Gerwins, Targeting the tumor stroma in hepatocellular carcinoma, World J. Hepatol. 7 (2) (2015) 165–176.

[12] M. Pieters, A.S. Wolberg, Fibrinogen and fibrin: an illustrated review, Res Pract Thromb Haemost 3 (2) (2019) 161–172.
[13] S. Thorsen, The mechanism of plasminogen activation and the variability of the fibrin effector during tissue-type plasminogen activator-mediated fibrinolysis, Ann. N. Y. Acad. Sci. 667 (1992) 52–63.
[14] J.B. Walker, M.E. Nesheim, The molecular weights, mass distribution, chain composition, and structure of soluble fibrin degradation products released from a fibrin clot perfused with plasmin, J. Biol. Chem. 274 (8) (1999) 5201–5212.
[15] G. Wu, A.J. Quek, T.T. Caradoc-Davies, S.M. Ekkel, B. Mazzitelli, J.C. Whisstock, R.H.P. Law, Structural studies of plasmin inhibition, Biochem. Soc. Trans. 47 (2) (2019) 541–557.
[16] C.A. Staton, N.J. Brown, C.E. Lewis, The role of fibrinogen and related fragments in tumour angiogenesis and metastasis, Expert. Opin. Biol. Ther. 3 (7) (2003) 1105–1120.
[17] C.L. Slade, S.V. Pizzo, L.M. Taylor Jr., H.M. Steinman, P.A. McKee, Characterization of fragment E from fibrinogen and cross-linked fibrin, J. Biol. Chem. 251 (6) (1976) 1591–1596.
[18] A. Saray, R. Mesihovic, S. Gornjakovic, N. Vanis, A. Mehmedovic, K. Nahodovic, S. Glavas, V. Papovic, Association between high D-dimer plasma levels and ascites in patients with liver cirrhosis, Medical Archives 66 (6) (2012) 372–374.
[19] I. Marie, J.Y. Borg, M.F. Hellot, H. Levesque, Plasma D-dimer concentration in patients with systemic sclerosis, Br. J. Dermatol. 158 (2) (2008) 392–395.
[20] H. Kubo, K. Nakayama, M. Yanai, T. Suzuki, M. Yamaya, M. Watanabe, H. Sasaki, Anticoagulant therapy for idiopathic pulmonary fibrosis, Chest 128 (3) (2005) 1475–1482.
[21] M. Naito, C.M. Stirk, E.B. Smith, W.D. Thompson, Smooth muscle cell outgrowth stimulated by fibrin degradation products. The potential role of fibrin fragment E in restenosis and atherogenesis, Thromb. Res. 98 (2) (2000) 165–174.
[22] M. Kodama, M. Naito, H. Nomura, A. Iguchi, W.D. Thompson, C.M. Stirk, E.B. Smith, Role of D and E domains in the migration of vascular smooth muscle cells into fibrin gels, Life Sci. 71 (10) (2002) 1139–1148.
[23] C.A. Bootle-Wilbraham, S. Tazzyman, W.D. Thompson, C.M. Stirk, C.E. Lewis, Fibrin fragment E stimulates the proliferation, migration and differentiation of human microvascular endothelial cells in vitro, Angiogenesis 4 (4) (2001) 269–275.
[24] M. Kang, R.A. Vaughan, C.M. Paton, FDP-E induces adipocyte inflammation and suppresses insulin-stimulated glucose disposal: effect of inflammation and obesity on fibrinogen Bbeta mRNA, Am. J. Physiol. Cell Physiol. 309 (11) (2015) C767–C774.
[25] H. Nomura, M. Naito, A. Iguchi, W.D. Thompson, E.B. Smith, Fibrin gel induces the migration of smooth muscle cells from rabbit aortic explants, Thromb. Haemost. 82 (4) (1999) 1347–1352.
[26] I. Barkefors, S. Le Jan, L. Jakobsson, E. Hejll, G. Carlson, H. Johansson, J. Jarvius, J.W. Park, N. Li Jeon, J. Kreuger, Endothelial cell migration in stable gradients of vascular endothelial growth factor a and fibroblast growth factor 2: effects on chemotaxis and chemokinesis, J. Biol. Chem. 283 (20) (2008) 13905–13912.
[27] S. Thorslund, H. Nguyen, T. Larang, I. Barkefors, J. Kreuger, A disposable and multifunctional capsule for easy operation of microfluidic elastomer systems, J. Micromech. Microeng. 21 (12) (2011).
[28] A.C. Ruifrok, D.A. Johnston, Quantification of histochemical staining by color deconvolution, Analytical and Quantitative Cytology and Histology / the International Academy of Cytology [and] American Society of Cytology 23 (4) (2001) 291–299.
[29] Y.H. Guo, I. Hernandez, B. Isermann, T.B. Kang, L. Medved, R. Sood, E.J. Kerschen, T. Holyst, M.W. Mosesson, H. Weiler, Caveolin-1-dependent apoptosis induced by fibrin degradation products, Blood 113 (18) (2009) 4431–4439.
[30] S.H. Kaufmann, S. Desnoyers, Y. Ottaviano, N.E. Davidson, G.G. Poirier, Specific proteolytic cleavage of poly(ADP-ribose) polymerase: an early marker of chemotherapy-induced apoptosis, Cancer Res. 53 (17) (1993) 3976–3985.
[31] S.T. Smiley, J.A. King, W.W. Hancock, Fibrinogen stimulates macrophage chemokine secretion through toll-like receptor 4, J. Immunol. 167 (5) (2001) 2887–2894.
[32] I. Sorensen, N. Susnik, T. Inhester, J.L. Degen, A. Melk, H. Haller, R. Schmitt, Fibrinogen, acting as a mitogen for tubulointerstitial fibroblasts, promotes renal fibrosis, Kidney Int. 80 (10) (2011) 1035–1044.
[33] M. Ii, N. Matsunaga, K. Hazeki, K. Nakamura, K. Takashima, T. Seya, O. Hazeki, T. Kitazaki, Y. Iizawa, A novel cyclohexene derivative, ethyl (6R)-6-[N-(2-Chloro-4-fluorophenyl)sulfamoyl]cyclohex-1-ene-1-carboxylate (TAK-242), selectively inhibits toll-like receptor 4-mediated cytokine production through suppression of intracellular signaling, Mol. Pharmacol. 69 (4) (2006) 1288–1295.
[34] E. Seki, S. De Minicis, C.H. Osterreicher, J. Kluwe, Y. Osawa, D.A. Brenner, R.F. Schwabe, TLR4 enhances TGF-beta signaling and hepatic fibrosis, Nat. Med. 13 (11) (2007) 1324–1332.
[35] M. Friedlander, P.C. Brooks, R.W. Shaffer, C.M. Kincaid, J.A. Varner, D.A. Cheresh, Definition of two angiogenic pathways by distinct alpha v integrins, Science (New York, N.Y.) 270 (5241) (1995) 1500–1502.
[36] J. Kolodziejczyk, M.B. Ponczek, The role of fibrinogen, fibrin and fibrin(ogen) degradation products (FDPs) in tumor progression, Contemp. Oncol. 17 (2) (2013) 113–119.
[37] I.A. van den Oever, N. Sattar, M.T. Nurmohamed, Thromboembolic and cardiovascular risk in rheumatoid arthritis: role of the haemostatic system, Ann. Rheum. Dis. 73 (6) (2014) 954–957.
[38] A. Ludwicka-Bradley, R.M. Silver, G.S. Bogatkevich, Coagulation and autoimmunity in scleroderma interstitial lung disease, Semin. Arthritis Rheum. 41 (2) (2011) 212–222.
[39] Y. Soma, K. Takehara, Y. Ishibashi, Alteration of the chemotactic response of human skin fibroblasts to PDGF by growth factors, Exp. Cell Res. 212 (2) (1994) 274–277.
[40] D. Onichtchouk, Y.G. Chen, R. Dosch, V. Gawantka, H. Delius, J. Massague, C. Niehrs, Silencing of TGF-beta signalling by the pseudoreceptor BAMBI, Nature 401 (6752) (1999) 480–485.
[41] Y. Fan, X. Li, W. Xiao, J. Fu, R.C. Harris, M. Lindenmeyer, C.D. Cohen, N. Guillot, M.H. Baron, N. Wang, K. Lee, J.C. He, D. Schlondorff, P.Y. Chuang, BAMBI elimination enhances alternative TGF-beta signaling and glomerular dysfunction in diabetic mice, Diabetes 64 (6) (2015) 2220–2233.
[42] C. Termeer, F. Benedix, J. Sleeman, C. Fieber, U. Voith, T. Ahrens, K. Miyake, M. Freudenberg, C. Galanos, J.C. Simon, Oligosaccharides of Hyaluronan activate dendritic cells via toll-like receptor 4, J. Exp. Med. 195 (1) (2002) 99–111.
[43] M. Yu, H. Wang, A. Ding, D.T. Golenbock, E. Latz, C.J. Czura, M.J. Fenton, K.J. Tracey, H. Yang, HMGB1 signals through toll-like receptor (TLR) 4 and TLR2, Shock 26 (2) (2006) 174–179.
[44] M.T. Campbell, K.L. Hile, H. Zhang, H. Asanuma, B.A. Vanderbrink, R.R. Rink, K.K. Meldrum, Toll-like receptor 4: a novel signaling pathway during renal fibrogenesis, J. Surg. Res. 168 (1) (2011) e61–e69.
[45] S. Bhattacharyya, K.S. Midwood, H. Yin, J. Varga, Toll-like Receptor-4 signaling drives persistent fibroblast activation and prevents fibrosis resolution in scleroderma, Adv Wound Care (New Rochelle) 6 (10) (2017) 356–369.
[46] S. Bhattacharyya, W. Wang, W. Qin, K. Cheng, S. Coulup, S. Chavez, S. Jiang, K. Raparia, L.M.V. De Almeida, C. Stehlik, Z. Tamaki, H. Yin, J. Varga, TLR4-dependent fibroblast activation drives persistent organ fibrosis in skin and lung, JCI Insight 3 (13) (2018).
[47] R.M. Kelsh-Lasher, A. Ambesi, C. Bertram, P.J. McKeown-Longo, Integrin alpha4-beta1 and TLR4 cooperate to induce fibrotic gene expression in response to Fibronectin's EDA domain, J Invest Dermatol 137 (12) (2017) 2505–2512.
[48] C. Freudlsperger, Y. Bian, S. Contag Wise, J. Burnett, J. Coupar, X. Yang, Z. Chen, C. Van Waes, TGF-beta and NF-kappaB signal pathway cross-talk is mediated through TAK1 and SMAD7 in a subset of head and neck cancers, Oncogene 32 (12) (2013) 1549–1559.
[49] P. Rameshwar, R. Narayanan, J. Qian, T.N. Denny, C. Colon, P. Gascon, NF-kappa B as a central mediator in the induction of TGF-beta in monocytes from patients with idiopathic myelofibrosis: an inflammatory response beyond the realm of homeostasis, J. Immunol. 165 (4) (2000) 2271–2277.
[50] W.W. Kilarski, B. Samolov, L. Petersson, A. Kvanta, P. Gerwins, Biomechanical regulation of blood vessel growth during tissue vascularization, Nat. Med. 15 (6) (2009) 657–664.
[51] F. El-Ayoubi, J. Amiral, J. Pascaud, S. Charrin, B. Tassel, G. Uzan, V. Gurewich, A fibrin antibody binding to fibronectin induces potent inhibition of angiogenesis, Thromb. Haemost. 113 (1) (2015) 143–153.
[52] H.F. Dvorak, Tumors: wounds that do not heal. Similarities between tumor stroma generation and wound healing, N. Engl. J. Med. 315 (26) (1986) 1650–1659.
[53] H.F. Dvorak, Tumors: wounds that do not heal-a historical perspective with a focus on the fundamental roles of increased vascular permeability and clotting, Semin. Thromb. Hemost. 45 (6) (2019) 576–592.
[54] S. Ahmad, A.A. Ansari, Therapeutic roles of heparin anticoagulants in cancer and related disorders, Med. Chem. 7 (5) (2011) 504–517.
[55] C.A. Spek, H.H. Versteeg, K.S. Borensztajn, Anticoagulant therapy of cancer patients: will patient selection increase overall survival? Thromb. Haemost. 114 (3) (2015) 530–536.
[56] L. Rosenberg, C. Louik, S. Shapiro, Nonsteroidal antiinflammatory drug use and reduced risk of large bowel carcinoma, Cancer 82 (12) (1998) 2326–2333.
[57] S.I. Schlager, S. Dray, Complete local tumor regression with antibody to fibrin fragment E, J. Immunol. 115 (4) (1975) 976–981.
[58] J.S. Palumbo, J.M. Potter, L.S. Kaplan, K. Talmage, D.G. Jackson, J.L. Degen, Spontaneous hematogenous and lymphatic metastasis, but not primary tumor growth or angiogenesis, is diminished in fibrinogen-deficient mice, Cancer Res. 62 (23) (2002) 6966–6972.
[59] H.H. Davila, M.G. Ferrini, J. Rajfer, N.F. Gonzalez-Cadavid, Fibrin as an inducer of fibrosis in the tunica albuginea of the rat: a new animal model of Peyronie's disease, BJU Int. 91 (9) (2003) 830–838.
[60] M.J. Flick, C.M. LaJeunesse, K.E. Talmage, D.P. Witte, J.S. Palumbo, M.D. Pinkerton, S. Thornton, J.L. Degen, Fibrin(ogen) exacerbates inflammatory joint disease through a mechanism linked to the integrin alphaMbeta2 binding motif, J. Clin. Invest. 117 (11) (2007) 3224–3235.